

Pit density reduction for AlN epilayers grown by molecular beam epitaxy using Al modulation method

Huan Liu(刘欢), Peng-Fei Shao(邵鹏飞), Song-Lin Chen(陈松林), Tao Tao(陶涛), Yu Yan(严羽), Zi-Li Xie(谢自力), Bin Liu(刘斌), Dun-Jun Chen(陈敦军), Hai Lu(陆海), Rong Zhang(张荣), and Ke Wang(王科)

Citation: Chin. Phys. B, 2024, 33 (**10**): 106801. DOI: 10.1088/1674-1056/ad7671
Journal homepage: http://cpb.iphy.ac.cn; http://iopscience.iop.org/cpb

What follows is a list of articles you may be interested in

Atomically self-healing of structural defects in monolayer WSe_2

Kangshu Li(李康舒), Junxian Li(李俊贤), Xiaocang Han(韩小藏), Wu Zhou(周武), and Xiaoxu Zhao(赵晓续)
Chin. Phys. B, 2024, 33 (**9**): 096804. DOI: 10.1088/1674-1056/ad641f

Microscopic growth mechanism and edge states of monolayer 1T'-$MoTe_2$

Haipeng Zhao(赵海鹏), Yin Liu(刘隐), Shengguo Yang(杨胜国), Chenfang Lin(林陈昉), Mingxing Chen(陈明星), Kai Braun, Xinyi Luo(罗心仪), Siyu Li(李思宇), Anlian Pan(潘安练), and Xiao Wang(王笑)
Chin. Phys. B, 2024, 33 (**4**): 046801. DOI: 10.1088/1674-1056/ad16d5

Growth and characterization of Bi(110)/$CrTe_2$ heterostructures: Exploring interplay between magnetism and topology

Zhenyu Yuan(袁震宇), Fazhi Yang(杨发枝), Baiqing Lv(吕佰晴), Yaobo Huang(黄耀波), Tian Qian(钱天), Jinpeng Xu(徐金朋), and Hong Ding(丁洪)
Chin. Phys. B, 2024, 33 (**2**): 026802. DOI: 10.1088/1674-1056/ad082a

Critical behavior in the epitaxial growth of two-dimensional tellurium films on $SrTiO_3$ (001) substrates

Haimin Zhang(张海民), Dezhi Song(宋德志), Fuyang Huang(黄扶旸), Jun Zhang(仉君), and Ye-Ping Jiang(蒋烨平)
Chin. Phys. B, 2023, 32 (**6**): 066802. DOI: 10.1088/1674-1056/acc80d

Visualizing interface states in In_2Se_3–WSe_2 monolayer lateral heterostructures

Da Huo(霍达), Yusong Bai(白玉松), Xiaoyu Lin(林笑宇), Jinghao Deng(邓京昊), Zemin Pan(潘泽敏), Chao Zhu(朱超), Chuansheng Liu(刘传胜), and Chendong Zhang(张晨栋)
Chin. Phys. B, 2023, 32 (**5**): 056803. DOI: 10.1088/1674-1056/acbaef

---

RAPID COMMUNICATION

Pit density reduction for AlN epilayers grown by molecular beam epitaxy using Al modulation method

Huan Liu(刘欢)[1], Peng-Fei Shao(邵鹏飞)[1,2], Song-Lin Chen(陈松林)[1], Tao Tao(陶涛)[1], Yu Yan(严羽)[1], Zi-Li Xie(谢自力)[1], Bin Liu(刘斌)[1], Dun-Jun Chen(陈敦军)[1], Hai Lu(陆海)[1,2], Rong Zhang(张荣)[1,2,3], and Ke Wang(王科)[1,2,†]

[1] *Jiangsu Provincial Key Laboratory of Advanced Photonic and Electronic Materials, School of Electronic Science and Engineering, Nanjing University, Nanjing* 210093, *China*
[2] *Hefei National Laboratory, Hefei* 230088, *China*
[3] *Xiamen University, Xiamen* 361005, *China*

(Received 5 July 2024; revised manuscript received 24 August 2024; accepted manuscript online 3 September 2024)

We have investigated homoepitaxy of AlN films grown by molecular beam epitaxy on AlN/sapphire templates by adopting both the continuous growth method and the Al modulation epitaxy (AME) growth method. The continuous growth method encounters significant challenges in controlling the growth mode. As the precise Al/N = 1.0 ratio is difficult to achieve, either the excessive Al-rich or N-rich growth mode occurs. In contrast, by adopting the AME growth method, such a difficulty has been effectively overcome. By manipulating the supply time of the Al and nitrogen sources, we were able to produce AlN films with much improved surface morphology. The first step of the AME method, only supplying Al atoms, is important to wet the surface and the Al adatoms can act as a surfactant. Optimization of the initial Al supply time can effectively reduce the pit density on the grown AlN surface. The pits density dropped from 12 pits/μm^2 to 1 pit/μm^2 and the surface roughness reduced from 0.72 nm to 0.3 nm in a 2×2 μm^2 area for the AME AlN film homoepitaxially grown on an AlN template.

Keywords: Al modulation epitaxy, molecular beam epitaxy, AlN, pits

PACS: 68.55.–a, 81.15.–z, 77.55.hd, 61.72.Ff **DOI:** 10.1088/1674-1056/ad7671

1. Introduction

AlN boasts numerous advantages, including a wide direct bandgap (6.2 eV), high saturation carrier drift velocity, exceptional thermal stability, high breakdown field strength, and high surface acoustic velocity. Furthermore, AlN exhibits similar lattice constants and thermal expansion coefficients to other III-nitride materials, making it the optimal substrate for deep ultraviolet (DUV) LEDs and other AlGaN based devices with high Al composition.[1–3] Its versatility renders it suitable for fabricating high-temperature, high-frequency, and high-power electronic devices, DUV optoelectronic devices, and surface acoustic wave devices.[4]

The high cost and limited availability of AlN single crystal substrates have considerably hindered their applications. Instead, AlN-on-sapphire template technologies have been developed quickly and are widely available nowadays. Such an AlN/sapphire template is a good starting platform to grow various fine heterostructures for device applications.[5] AlN epilayers on an AlN/sapphire template can be obtained by various methods, mainly, metal–organic chemical vapor deposition (MOCVD), hydride vapor phase epitaxy (HVPE), and molecular beam epitaxy (MBE).[6] MBE offers unique advantages owing to its ultra-clean and ultra-high vacuum environment, which effectively minimizes parasitic reactions and hydrogen passivation effects usually observed in MOCVD reactors.[7] Furthermore, MBE enables precise control over shutter operations, facilitating the realization of complex structures and sharp heterogeneous interfaces.[8]

The growth mode of AlN is similar to that of GaN, and is characterized by N-rich growth, slightly Al-rich growth, and excessive Al-rich growth, depending on the Al supply.[9,10] Consequently, the Al/N ratio influences the quality of AlN films significantly. AlN films grown in the N-rich region exhibit a rough three-dimensional (3D) surface morphology and poor crystal quality. Conversely, films grown in the slightly Al-rich region feature a smoother surface morphology and improved crystal quality. However, excessive Al-rich growth leads to the formation of numerous metal droplets on the growth front.[11] To circumvent the formation of Al droplets, researchers have employed three primary methods. Firstly, the high-temperature desorption (1150 °C or above) removes excessive Al droplets effectively.[12,13] However, this method exceeds the growth temperature range of usual MBE systems. Secondly, the N radical beam irradiation reacts with excessive Al droplets to form crystals.[14] Thirdly, the metal-modulated epitaxy (MME) method has been utilized.[15–17] For instance, Burnham *et al.* used the MME method to open the Al and N

†Corresponding author. E-mail: kewang@nju.edu.cn
© 2024 Chinese Physical Society and IOP Publishing Ltd

sources alternately, and this method enhances lateral growth and eliminates excessive Al droplets.[16] However, apart from AlN grown at particularly high temperatures, conventional temperature (1000 °C) MBE growth of AlN films often suffers from a high density of surface pits. Nakajima *et al.* demonstrated that the pit density strongly depended on the residual impurities of the MBE chamber, and by reducing impurity (O, OH, and H_2O), the pit density was reduced.[18]

In this paper, we have conducted homogeneous epitaxy of AlN films by MBE on AlN/sapphire templates using two different growth methods, continuous epitaxy method and Al modulation epitaxy (AME) method. Based on the surface morphology of AlN films grown by conventional method, we found that it is difficult to control the growth mode of AlN film, resulting in the appearance of either pits or Al droplets on the film surface. Subsequently, we employed the AME method, which significantly reduced the density, depth, and diameter of pits. Finally, we achieved nearly pit-free AlN films grown by AME method.

2. Experimental procedures

The experiments were carried out using a RIBER Compact 21 PA-MBE system equipped with evaporation sources for several group III metals (Al, Ga and In) and a nitrogen plasma source. All samples were grown on 4.5 μm thick C-plane AlN/sapphire templates grown by MOCVD. An approximately 500 nm thick molybdenum layer was deposited on the back side of the AlN/sapphire template to absorb heat. The AlN templates were sequentially washed with acetone, ethanol, deionized water, and etched in HCl before being loaded into the MBE chamber. Prior to growth, the AlN templates were degassed in degas chamber at 450 °C for approximately 1.5 hour. The N_2 plasma (N^*) conditions were fixed at nitrogen flow rate of 0.7 standard cubic centimeter per minute (SCCM) and radio frequency power of 450 W. Reflection high-energy electron diffraction (RHEED) patterns and intensity were collected by the KSA400 system equipped with a CCD camera and a frame collector. The growth temperature was monitored by a thermal couple in the MBE system.

For the continuous epitaxial method, the Al and N^* shutters are open continuously during the whole growth process. In contrast, one AME cycle is divided into three steps, as shown in Fig. 1. During step I, only the Al source shutter is opened to supply some Al atoms, which is important to wet the surface and the Al adatoms can act as a surfactant. During step II, both Al and N^* shutters are opened to grow AlN films. During step III, the Al shutter is closed and only N^* shutter is opened to consume the excessive Al and grow AlN films. Because the thermal evaporation rate of Al atoms is very low at relatively low temperature, excessive Al atoms can easily accumulate to form Al droplets. In order to consume the excessive Al droplets, the Al source shutter is switched off and the N^* is opened to consume the excessive Al.[17] Finally, AlN films with smoother surface morphology can be obtained.

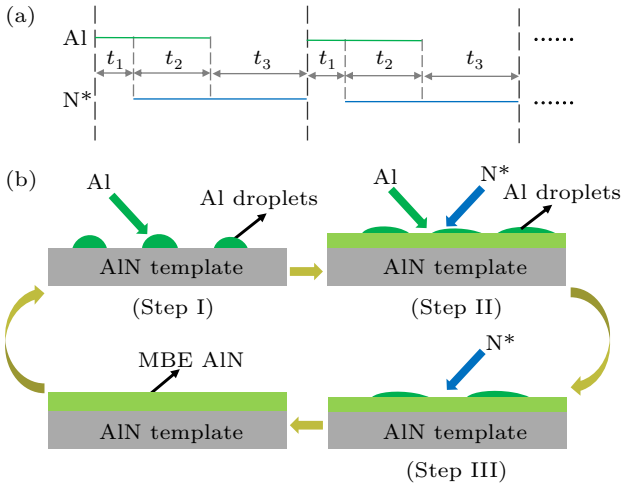


Fig. 1. AME schematic diagram, the Al and N plasma shutter time sequence (a) and the AME method schematic diagram (b) to illustrate the three steps in one AME cycle. During step I, only the Al source shutter is opened to supply some Al atoms. During step II, both Al and N^* shutter are opened to grow AlN films. During step III, Al shutter is closed and only N^* shutter is opened to consume the excessive Al and grow AlN films.

Samples A, B, and C were grown by the continuous growth method. Samples D, E, F, and G were grown by the AME growth method. The detailed growth parameters for all samples are presented in Table 1. Growth progress was monitored *in-situ* by RHEED,[19] and RHEED pattern and intensity were recorded during growth. The surface morphology of the samples was characterized by atomic force microscopy (AFM) and optical microscope (OM).

Table 1. Growth parameters of samples.

Sample number	Substrate temperature (°C)	Al flux (Torr)	N^* flow (sccm)	Al supply time t_1 (s)	AlN growth time t_2 (s)	N^* consume time t_3 (s)	Film thickness (nm)
A	970	1.3×10^{-7}	0.7		conventional growth		160
B	970	1.4×10^{-7}	0.7		conventional growth		160
C	970	1.6×10^{-7}	0.7		conventional growth		160
D	970	1.4×10^{-7}	0.7	18	60	48	144
E	970	1.4×10^{-7}	0.7	24	60	60	160
F	970	1.4×10^{-7}	0.7	30	60	72	176
G	970	1.4×10^{-7}	0.7	36	60	84	192

3. Results and discussion

3.1. Continuous epitaxy of AlN film

Figure 2 shows the results of three samples grown by continuous epitaxy method with different Al fluxes at 970 °C. The Al fluxes of samples A, B, and C are 1.3×10^{-7} Torr, 1.4×10^{-7} Torr, and 1.6×10^{-7} Torr, respectively. As shown in Fig. 2(a′), the morphology of sample A is typical of the N-rich mode growth. It has an extremely rough surface with large pits, and the RMS as high as 2.9 nm in a 2×2 μm^2 area. Figure 2(a) shows the OM image of N-rich condition, there are no Al droplets. Because there are no excessive Al atoms that act as surfactant, the mobility of the Al atoms is extremely low, pit appears at the ends of the spiral dislocations.[20] Moreover, as shown in Fig. 2(a″), the RHEED pattern also shows a typical dotted line pattern of N-rich mode growth. It is similar to the results of the GaN N-rich mode.[10] The Al flux is increased to 1.4×10^{-7} Torr for sample B, which is the slightly Al-rich condition. As shown in Fig. 2(b″), the RMS drops significantly to 0.5 nm in a 2×2 μm^2 area. Figure 2(b″) also shows that the intensity of the RHEED pattern increases, bright and streaky. However, as shown in Fig. 2(b), some Al droplets can be seen on the surface. Moreover, some hexagonal hillocks and some pits can be seen in Fig. 2(b′). The Al flux is increased to 1.6×10^{-7} Torr for sample C, which is the excessive Al-rich condition. Figure 2(c′) shows that sample C has a higher RMS of 1.2 nm in a 2×2 μm^2 area, presents a large number of Al droplets, and is accompanied by some pits. As shown in Fig. 2(c″), a dark RHEED pattern is observed, indicating metal coverage and reduced electron diffraction.[17,21] The above results illustrate that it is difficult to control the AlN films growth mode precisely using continuous epitaxy method, either the excessive Al-rich or N-rich growth mode occurs. Moreover, in continuous epitaxy under slightly Al-rich condition, growth surfaces still show pits and hexagonal Al hillocks formed by small amounts of Al droplets.[17]

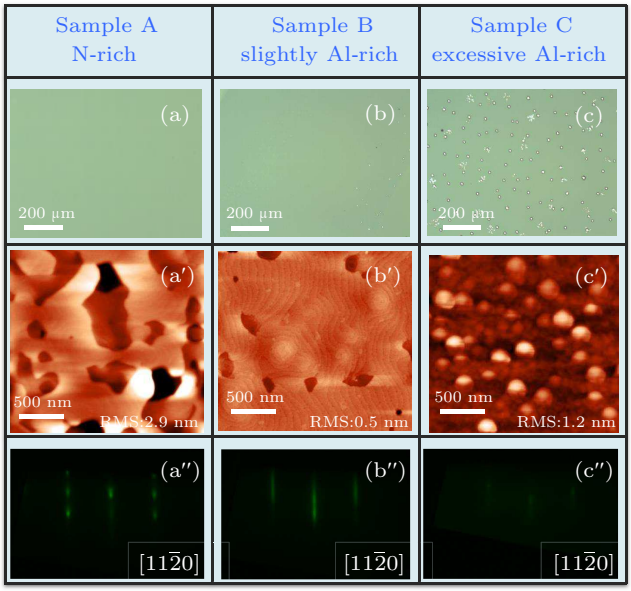


Fig. 2. OM images (first row), AFM images (second row) in a 2×2 μm^2 area and [11$\bar{2}$0] directional RHEED patterns of AlN films grown by continuous epitaxy method with different Al fluxes of 1.3×10^{-7} Torr, 1.4×10^{-7} Torr and 1.6×10^{-7} Torr, respectively.

3.2. Al modulation epitaxy of AlN film

For the epitaxial growth of arsenides such as conventional GaAs/AlGaAs, the migration enhanced epitaxy (MEE) method was proposed and often used in the 1980s, using alternating anionic (As) and cationic (Ga or Al) shutters to enhance the migration of cations.[22] The mechanism is that cations are highly reactive with anions, and in the absence of anions, the surface diffusion length of cations becomes longer,[16] i.e., the migration ability is enhanced and the film quality is improved. In the case of MBE epitaxial growth of group III nitrides, it is different. Extensive experimental and theoretical analyses have shown that the excess of Ga or In adlayers can act as a surfactant,[23–26] since the adsorbed metal layer on the surface of the nitride semiconductor possesses the properties of a partially mobile liquid, which can provide a lateral migration channel for the nitrogen atoms.[27] Such surfactant effect can enhance the migration ability of each atom and thus facilitate group III nitride growth. MBE epitaxy of AlN has similar effects, and some works using the AME method have been able to improve the crystal quality to some extent.[28–30] In this work, some Al was supplied to the growth front at the first step of each AME AlN growth cycle, which is expected to enhance the migration of atoms on the surface of the film and strengthen the lateral growth.

Figure 3(a) shows the typical RHEED intensity variation for a cycle of epitaxial samples D, E, F and G with various Al supply time using AME method. The initial Al supply time of samples D, E, F, and G is 18 s, 24 s, 30 s, and 36 s, respectively. Both Al and N* sources are supplied simultaneously for 60 s for all samples. The main difference is the separate supply time of Al source and N* source. Detailed growth parameters can be found in Table 1. Based on the overall variation of the RHEED intensity curves in Fig. 3(a), one cycle of the AME consists of three-time stages t_1, t_2, and t_3, corresponding to steps I, II, and III in Fig. 1. In the first step, the RHEED intensity gradually decreases with the opening time of the Al source shutter increasing, as the Al adatom reduces the diffraction intensity of electrons, and causes the RHEED intensity to drop to the minimum value approximately. In the second step, both Al source and N* source shutters are opened for about 60 s, the RHEED intensity remains almost constant and is approximately equal to the minimum value at the end of the first step. In the third step, the Al source shutter is closed quickly and the N* source continues to be supplied. The RHEED intensity initially remains at the level of the second step for τ_1 time

and then rises in τ_2 time to approximately the intensity before the first step. Notably, figure 3(a) shows that as the t_1 time increases, τ_1 also increases gradually, showing a pattern of t_1 increasing by 6 s for every 12 s increase in τ_1. However, the τ_2 time is almost unchanged for about 20 s. Since the excessive Al on the growth surface can provide sufficient Al atoms to maintain two monolayers (MLs) of Al atoms and some Al droplets, τ_1 is only related to the amount of Al droplets on the surface, and τ_2 is only related to the consumption of two MLs Al atoms by N* treatment. The two MLs Al coverage behavior is evidenced in the Al adatom adsorption/desorption experiments with different beam fluxes at various temperatures, which will be published elsewhere, and similar behaviors of Ga and In adatoms have been demonstrated before.[31–33] Consequently, the τ_2 time is almost unchanged, about 20 s. We believe that a long t_1 time can cause a large residue of Al atoms, which may appear as Al droplets after growth. But the N* source can consume excessive Al atoms during step III. As the Al source has been closed before step III, it will take less time for N* to consume the excessive Al atoms. Consequently, we find that periodic closing of the Al and N* sources is necessary to check whether the N* treatment consumes excessive Al can obtain a smoother AlN film.

Figures 3(b)–3(e) show RHEED patterns evolution at different times (t_1, t_2, τ_1 and τ_2) of sample F in one AME cycle. Figure 3(b) shows that the RHEED pattern with only Al atoms supplied is relatively dark, and as the time of supplying Al atoms increases, as shown in Fig. 3(c), the RHEED pattern becomes even darker until the state at time t_2. Because the Al metal will cover the surface and reduce the electron diffraction, similar to the RHEED pattern during AlN growth. As shown in Fig. 3(e), until entering t_3 time (τ_1 and τ_2), N* is supplied alone and the RHEED pattern gradually turns into bright streaks.

Figure 4 shows the OM images, AFM images and [11$\bar{2}$0] direction RHEED patterns of samples D, E, F and G fabricated by the AME method. In Figs. 4(a)–4(d), as the Al supply time increases, sample D has some black spots, sample E has fewer black spots, sample F has almost no black spots, however, sample G shows some black spots again. It means that the morphology gets better then worse with the increase of the Al supply time. Figures 4(a′)–4(d′) show the AFM images of samples D, E, F and G. It can be seen that the RMS value of AlN film decreases from 0.72 nm to 0.3 nm in a 2×2 μm^2 area and then increases to 0.5 nm gradually as the Al supply time increases. As shown in Figs. 4(a″)–4(d″), the RHEED pattern streaks become clearer and brighter as the Al supply time increases, except for sample G. It indicates that a better homogeneous epitaxial growth has been achieved. Conversely, sample G has a darker stripe pattern, which may be due to excessive Al supply time. Excessive Al metal can cover the surface and reduce the electron diffraction.

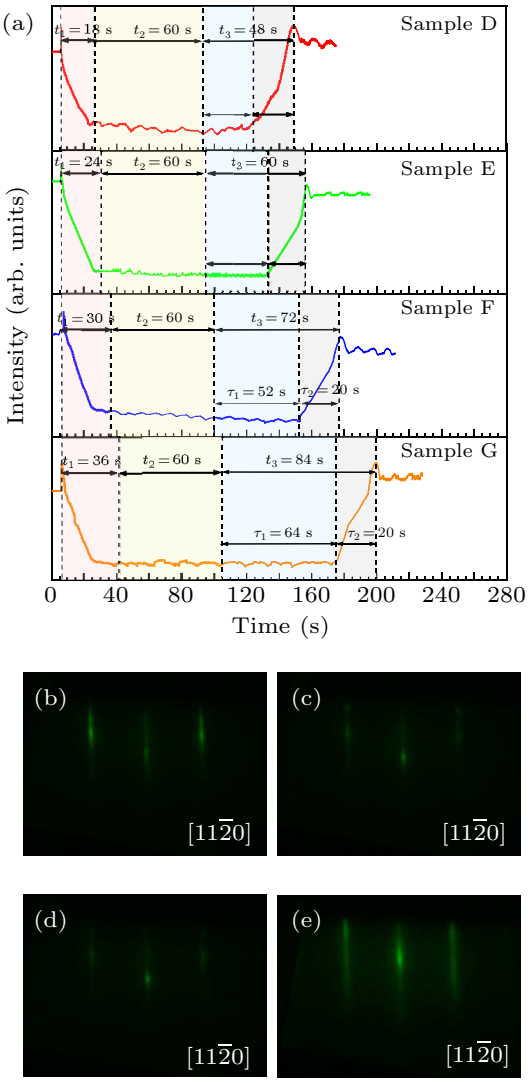


Fig. 3. The RHEED spectra intensity comparison of one cycle AME method for samples D, E, F, and G with various Al supply time of 18 s, 24 s, 30 s, and 36 s, respectively (a), and the RHEED patterns evolution at different time (t_1, t_2, τ_1, and τ_2) of sample F in one AME cycle (b)–(e).

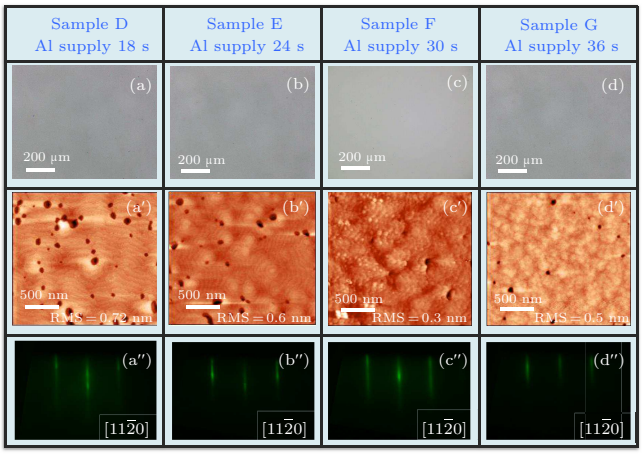


Fig. 4. OM images (first row), AFM images (second row) in a 2×2 μm^2 area and [11$\bar{2}$0] directional RHEED patterns of samples D, E, F, and G grown by AME method with various Al supply time of 18 s, 24 s, 30 s, and 36 s, respectively.

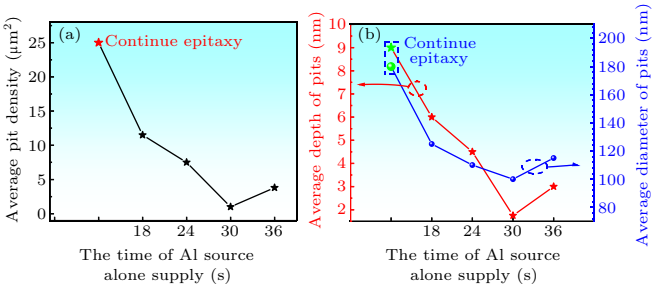


Fig. 5. The pit density (a) and average depth and diameter of the pit (b) for samples D, E, F and G with various Al supply time and samples of continue epitaxy. All data were extracted from Figs. 4(a′)–4(d′) and 2(a′)–2(c′).

The average pit density, average depth and diameter data of samples D, E, F, G and samples of continue epitaxy are extracted from the AFM images of Figs. 4(a′)–4(d′) and 2(a′)–2(c′), and are presented in Fig. 5. As shown in Fig. 5(a), the average pit density significantly decreases from 25 pit/μm^2 to 1 pit/μm^2 and then increases to approximate 3 pits/μm^2. Notably, sample F has the smallest average pit density, average pit depth and diameter, indicating that the surface morphology of AlN films is improved significantly, the pits could be significantly reduced using the AME method. These results align with variations observed in the RHEED patterns and OM images in the first row and second row of Fig. 4, confirming the efficacy of the AME method in optimizing the surface morphology of AlN films.

As shown in Fig. 6, we also did the x-ray diffraction (XRD) test [(a) the 2θ–ω, (b) [0002] direction x-ray rocking curves (XRCs), and (c) [10$\bar{1}$2] direction XRCs of AME AlN, continue epitaxy AlN and AlN template]. We found that the results of both continue epitaxy AlN and AME AlN are basically the same as those of AlN templates. Because MBE epitaxial AlN films were grown on AlN templates, which are as thick as 3–5 μm, which would seriously affect the XRD test results, and it is possible that the test information is all about the AlN templates. Moreover, we did the transmission electron microscope (TEM) test. As shown in Fig. 7 [(a) the cross-sectional many-beam dark-field image along the [0002] direction near the continue epitaxy AlN/MOCVD AlN interface and (b) the AME AlN/MOCVD AlN interface]. It can be seen that there are more defects at the interface of continue epitaxy AlN and MOCVD AlN, as shown in the red dashed circle of Fig. 7(a), while there are fewer defects at the interface of AME AlN and MOCVD AlN. Consequently, the AME growth method has some advantages.

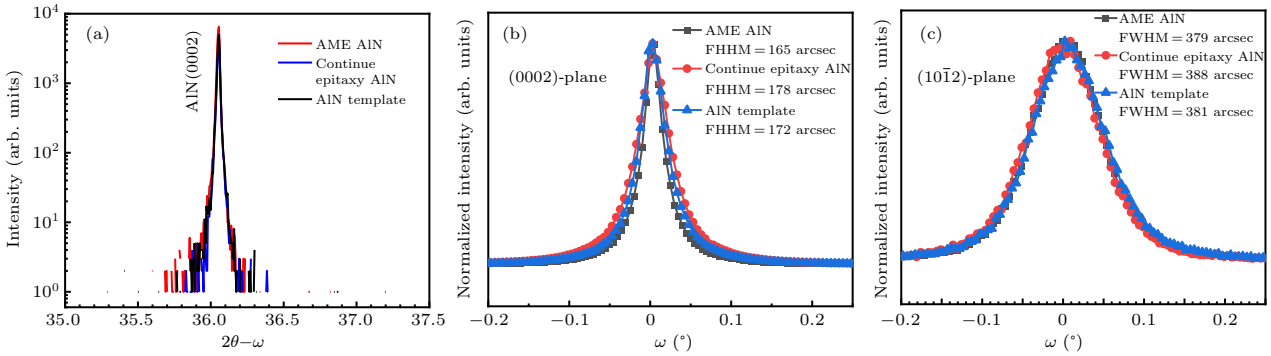


Fig. 6. The XRD [0002] 2θ–ω scan (a), [0002] rocking curves (b), and [10$\bar{1}$2] rocking curves (c) of AlN template, continue epitaxy AlN and AME AlN.

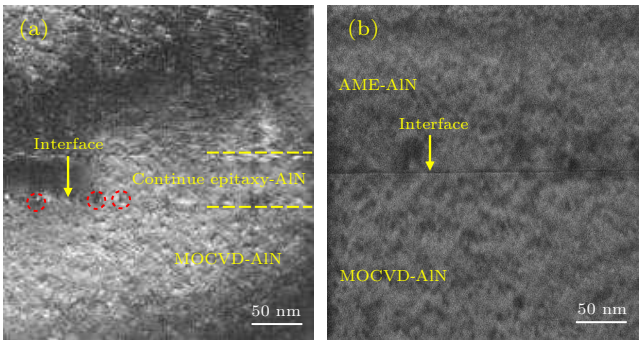


Fig. 7. TEM analysis of near the MBE AlN/MOCVD AlN interface. The cross-sectional many-beam dark-field images along the [0002] direction (a) near the continue epitaxy AlN/MOCVD AlN interface and (b) near the AME AlN/MOCVD AlN interface.

As shown in Fig. 8, we did the TEM test and the energy dispersive x-ray (EDX) spectroscopy test for AME AlN epilayer. From Fig. 8(b), it can be seen that the atom arrangement near the interface is more uniform, which indicates that the epitaxial quality is better. As shown in Figs. 8(c)–8(e), the Al and N elements near the interface are also uniformly distributed. It is implied that the Al/N atomic ratio of AME AlN and MOCVD AlN is less different, and only extremely small amounts of O elements are present at the interface. However, precise quantitative measurement of atomic ratio is more difficult, the EDX test is more accurate for heavy metal elements, such as the Al/Ga ratio in AlGaN. Consequently, the Al/N ratio we measured is just an estimation and can be used as a reference.

It was estimated that the amount of Al supply was about 3.6 MLs and 4.8 MLs for samples D and E in the step I of AME, respectively. The results have suggested that such amount of Al supply and the corresponding Al adlayers may not be enough to form a complete wetting layer on the growth

front, which in turn leads to incomplete transverse migration channels for nitrogen atoms. Consequently, there are more pits on the surfaces of samples D and E. As shown in Figs. 4(a″) and 4(b″), the RHEED pattern streaks show slight signs of dotted lines. In contrast, the amount of Al supply for sample G was 7.2 MLs in the step I of the AME. We suspect that it is too much so that the excessive Al atoms form Al droplets on top of the complete wetting layer, which deteriorates the morphology of sample G. The Al supply of sample F was 6 MLs in the step I of the AME, which probably formed a complete wetting layer and lateral migration channels for nitrogen atoms, and at the same time avoided Al droplet formation. Thus, better surface morphology is obtained at the end.

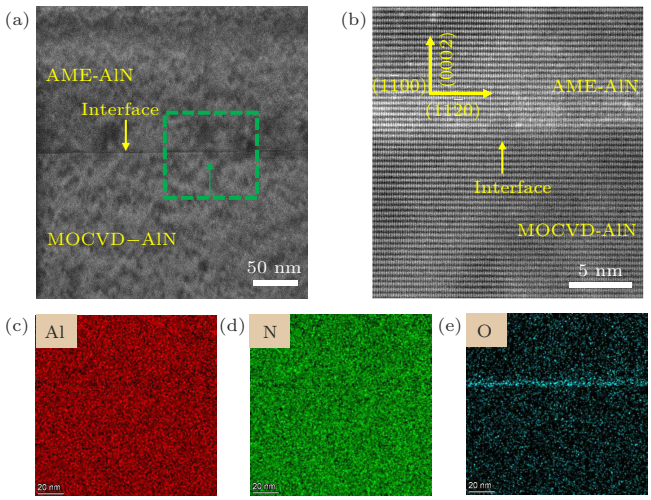


Fig. 8. TEM analysis of near the AME AlN/MOCVD AlN interface. (a) The cross-sectional many-beam dark-field image along the [0002] direction near the AME AlN/MOCVD AlN interface. (b) High resolution HAADF-STEM image in [11$\bar{2}$0] AlN zone axis of an interface between the AME AlN and MOCVD AlN. (c)–(e) EDX spectroscopy of Al, N, and O elements within the green dashed box area in panel (a).

4. Conclusion

The continuous AlN epitaxy growth method encounters significant challenges in precisely controlling growth mode at the usual growth temperature, either the excessive Al-rich or N-rich growth mode occurs. Excessive Al-rich growth leads to the formation of numerous metal droplets on the growth surface, and AlN films grown in the N-rich region exhibit a rough 3D surface morphology. By adopting AME growth method, we were able to produce AlN films with much improved surface morphology. The pits density dropped from 12 pits/μm^2 to approximate 1 pit/μm^2. And the surface roughness reduced from 0.72 nm to 0.3 nm in a 2×2 μm^2 area. The first step of the AME method, only supplying Al atoms, is important to wet the surface and the Al adatoms can act as a surfactant. Optimization of the initial Al supply time effectively reduces the pit density on the surface of the AlN films. The homo-epitaxy of AlN has established a foundation for the subsequent epitaxial growth of complex hetero-structures on an AlN template or a bulk AlN substrate.

Data availability statement

The data that support the findings of this study are openly available in Science Data Bank at the following link https://doi.org/10.57760/sciencedb.j00113.00134

Acknowledgments

Project supported by the Innovation Program for Quantum Science and Technology (Grant No. 2021ZD0303400), the National Key R&D Program of China (Grant No. 2022YFB3605602), the Key R&D Program of Jiangsu Province (Grant Nos. BE2020004-3 and BE2021026), the National Naturaal Science Foundation of China (Grant No. 61974065), and Jiangsu Special Professorship, Collaborative Innovation Center of Solid-State Lighting and Energy-saving Electronics.

References

[1] Melo E G and Alayo M I 2015 *Photonics and Nanostructures-Fundamentals and Applications* **14** 35
[2] Wang C, Gao X D, Li D D, Chen J J, Chen J F, Dong X M, Wang X D, Huang J, Zeng X H and Xu K 2023 *Chin. Phys. B* **32** 026802
[3] Pan D, Song H D, Zhang S, Liu L, Wen L J, Liao D Y, Zhuo R, Wang Z C, Zhang Z T and Yang S 2022 *Chin. Phys. Lett.* **39** 058101
[4] Bondokov R T, Mueller S G, Morgan K E, Slack G A, Schujman S, Wood M C and Schowalter L J 2008 *J. Cryst. Growth* **310** 4020
[5] Fukuyama H, Miyake H, Nishio G, Suzuki S and Hiramatsu K 2016 *Jpn. J. Appl. Phys.* **55** 5S
[6] Zhao L, Yang K, Ai Y, Zhang L, Niu X, Lv H and Zhang Y 2018 *Journal of Materials Science: Materials in Electronics* **29** 13766
[7] Nakarmi M L, Cai B, Lin J Y and Jiang H X 2012 *Phys. Status Solidi A* **209** 126
[8] Wu Y Z, Liu B, Li Z H, Tao T, Xie Z L, Xiu X Q, Chen P, Chen D J, Lu H, Shi Y and Zhang R 2019 *J. Cryst. Growth* **506** 30
[9] Heying B, Averbeck R, Chen L F, Haus E, Riechert H and Speck J S 2000 *Appl. Phys.* **88** 1855
[10] Li Z H, Shao P F, Shi G J, Wu Y Z, Wang Z P, Li S Q, Zhang D Q, Tao T, Xu Q J, Xie Z L, Ye J D, Chen D J, Liu B, Wang K, Zheng Y D and Zhang R 2022 *Chin. Phys. B* **31** 018102
[11] Kaneko M, Hirai K, Kimoto T and Suda J 2020 *Appl. Phys. Express* **13** 025503
[12] Cho Y J, Chang C S, Lee K, Nomoto K, Toita M, Schowalter L, Muller D A and Jena D 2020 *Appl. Phys. Lett.* **116** 172106
[13] Lee K, Cho Y J, Schowalter L J, Toita M, Xing H G and Jena D 2020 *Appl. Phys. Lett.* **116** 262102
[14] Yamaguchi T, Uematsu N, Araki T, Honda T, Yoon E and Nanishi Y 2013 *Cryst. Growth* **377** 123
[15] Burnham S D, Henderson W and Doolittle W A 2008 *Phys. Status Solidi C* **5** 1855
[16] Burnham S D, Namkoong G, Lee K K and Doolittle W A 2007 *J. Vac. Sci. Tech. B* **25** 3
[17] Shao P F, Li S Q, Li Z H, Zhou H, Zhang D Q, Tao T, Yan Y, Xie Z L, Wang K, Chen D J, Liu B, Zheng Y D, Zhang R, Tsungtse L, Wang L and Hirayama H 2022 *J. Phys. D: Appl. Phys.* **55** 364002
[18] Nakajima A, Furukawa Y, Koga S and Yonezu H 2004 *J. Cryst. Growth* **265** 351
[19] Li Z H, Shao P F, Wu Y Z, Shi G J, Tao T, Xie Z L, Chen P, Zhou Y G, Xiu X Q, Chen D J, Liu B, Wang K, Zheng Y D, Zhang R, Tsungtse L, Wang L and Hirayama H 2021 *Jpn. J. Appl. Phys.* **60** 075504
[20] Nechaev D V, Koshelev O A, Ratnikov V, Brunkov P N, Myasoedov A V, Sitnikova A, Ivanov S V and Jmerik V N 2020 *Superlattice Microst.* **138** 106368
[21] Koblmüller G, Brown J, Averbeck R, Riechert H, Pongratz P and Speck J S 2005 *Jpn. J. Appl. Phys.* **44** L906

[22] Horikoshi Y, Kawashima M and Yamaguchi H 1987 *Appl. Phys. Lett.* **50** 1686
[23] Northrup J E, Neugebauer J, Feenstra R M and Smith A R 2000 *Phys. Rev. B* **61** 9932
[24] Heying B, Smorchkova I, Poblenz C, Fini P, Denbaars S, Mishra U and Speck J S 2000 *Appl. Phys. Lett.* **77** 2885
[25] Koblmüller G, Averbeck R, Riechert H and Pongratz P 2004 *Phys. Rev. B* **69** 35325
[26] Neugebauer J, Zywietz T K, Scheffler M, Neugebauer, Northrup J E, Chen H J and Feenstra R M 2003 *Phys. Rev. Lett.* **90** 56101
[27] Koshelev O A, Dmitrii V N and Pavel N B 2021 *Semicond. Sci. Technol.* **36** 035007
[28] Nechaev D V, Aseev P A and Jmerik V N 2013 *J. Cryst. Growth* **378** 319
[29] Nilsson D, Janzén E and Kakanakova G A 2016 *J. Phys. D: Appl. Phys.* **49** 175108
[30] Dinh D V, Hu N, Honda Y, Amano H and Markus P 2018 *J. Cryst. Growth* **498** 377
[31] Christoph A, Julien B, Guido M and Bruno D 2003 *Phys. Rev. B* **67** 165419
[32] Gallinat C S, Koblmueller G, Brown J S and Speck J S 2007 *J. Appl. Phys.* **102** 064907
[33] Feenstra R M, Dong Y and Lee C D 2005 *J. Vac. Sci. Tech. B* **23** 1174